Will's new version of abstract

4 June 2016

ABSTRACT

In order to study the nature, origin, and impact of turbulent velocity fluctuations in the ionized gas of the Orion Nebula, we apply a variety of statistical techniques to observed velocity cubes. The cubes are derived from high resolving power ($R \approx 40\,000$) longslit spectroscopy of optical emission lines spanning a range of ionizations and covering the central $3' \times 5'$ of the nebula. From Velocity Channel Analysis (VCA), we find that the slope of the velocity power spectrum is consistent with predictions of Kolmogorov theory between scales of 8 and 22 arcsec (0.02 to 0.05 pc). The outer scale, which is the dominant scale of density fluctuations in the nebula, approximately coincides with the autocorrelation length of the velocity fluctuations that we determine from the second order velocity structure function. We propose that this is the principal driving scale of the turbulence, which originates in the autocorrelation length of dense cores in the Orion molecular filament. By combining analysis of the non-thermal line widths with the systematic trends of velocity centroid versus ionization, we find that the global champagne flow and smaller scale turbulence each contribute in equal measure to the total velocity dispersion, with respective RMS widths of 4–5 km s^{-1}. The turbulence is subsonic and can account for only one half of the derived variance in ionized density, with the remaining variance provided by density gradients in photoevaporation flows from globules and filaments.

4.3 What is the significance of the 22 arcsec and 8 arcsec length scales?

The velocity channel analysis suggests that two length scales are important in the Orion Nebula, corresponding to the limits of regime II (see Fig. 5). The break in power law at 22 arcsec and 8 arcsec occurs for both thin and thick velocity slices. This indicates that it is a feature of the emissivity power spectrum, and not the velocity power spectrum. Below 8 arcsec (regime III), the emissivity power spectrum is very steep in all the lines, indicating that small-scale fluctuations are relatively unimportant. Above 22 arcsec (regime I), the power spectrum $P(k)$ is very flat, similar to the noise-dominated spectrum in regime IV, suggesting that fluctuations are relatively uncorrelated on larger scales. This is underlined by the analysis in Appendix E, where it is shown that a combination of Gaussian brightness peaks with widths (FWHM) from $\approx 4''$ and $12''$ can capture the broad features of the observed power spectra.

The outer scale of $22''$ coincides with scale where the structure functions reach a value of unity (Fig. 8), which corresponds to the correlation length, l_0, of the velocity fluctuations (see Fig. 14). It is therefore plausible to associate this scale, which corresponds to a physical size of ≈ 0.05 parsec, with the driving scale of turbulence in the nebula. The inner scale of $8''$, corresponding to a physical size of ≈ 0.02 parsec, is harder to associate with any particular process since the structure functions (Fig. 8) show no apparent feature at this scale.

4.4 Does velocity turbulence cause the surface brightness fluctuations?

The surface brightness fluctuations on the plane of the sky are primarily caused by emissivity fluctuations within the nebular volume, which are in turn caused by fluctuations in electron density, temperature, and ionization. The temperature and ionization dependence of the emissivity is very different for each line, but the electron density dependence is similar in all cases, being $\propto N_e^2$ in the low density limit, which is appropriate for all but the [S II] lines. It therefore seems likely that any *commonalities* in the power spectra between all the different emission lines will give us information about the electron density fluctuations within the nebula.

In § **??** it was shown that the rms fractional surface brightness variation in 2D is $\sigma_{S/S_0} \approx 0.5$ for all lines, and the rms emissivity variation in 3D is predicted to be $\sigma_{E/E_0} = \xi \sigma_{S/S_0}$, where the "de-projection factor" is $\xi = 2$–3 (Brunt et al. 2010). On the other hand, if the emissivity fluctuations are due to variations in the density squared, then the rms fractional 3D density variation is $\sigma_{\rho/\rho_0} = 0.5\,\sigma_{E/E_0}$, which approximately cancels out the de-projection factor so that $\sigma_{\rho/\rho_0} \approx \sigma_{S/S_0} \approx 0.5$. If the density fluctuations are *caused* by the turbulent velocity fluctuations, then numerical simulations (Konstandin et al. 2012) show that there is a linear relationship between σ_{ρ/ρ_0} and the rms Mach number, M, of the turbulence: $\sigma_{\rho/\rho_0} = bM$, where $b = 1/3$ to $b = 1$, depending on whether the turbulent driving is primarily solenoidal or compressive. The rms Mach number is the ratio of the velocity dispersion to the ionized isothermal sound speed $M = \sigma_u / c_i$, where $\sigma_u = \sigma_{\rm turb} \approx 4$ km s^{-1} (see § 3.4) and $c_i \approx 11$ km s^{-1}. Thus, $M \approx 0.35$ so that, given $b < 1$, an upper limit to the turbulent contribution to the density fluctuations is $\sigma_{\rho/\rho_0} \lesssim 0.35$.

Furthermore, the slopes of the surface brightness fluctuation spectra in regime II are significantly shallower than expected from a top-down turbulent cascade in the subsonic limit (Konstandin et al. 2015). A similar result is seen in our numerical simulations (see § 4.2), with the important difference that in the simulation the ve-

locity spectrum is also shallow, whereas the thin-slice VCA analysis for the observations (§ 3.3.1) is consistent with a Kolmogorov slope for the velocity fluctuation spectrum in regime II.

We therefore require a further mechanism to explain the roughly 50% of the variance in ionized density that cannot be accounted for by turbulent velocity fluctuations. This could plausibly be provided by the bright-rimmed structure of the photoevaporation flows away from dense molecular globules and filaments (e.g., (Bertoldi & McKee 1990; Henney et al. 2009)), which are responsible for driving the turbulence. We have calculated the emissivity-weighted density PDF for a simple model of a single spherically divergent, isothermal evaporation flow from a D-critical ionization front (Dyson 1968) and find $\sigma_{\rho/\rho_0} = 0.56$. For an an ensemble of such flows with varying peak densities the σ_{ρ/ρ_0} would be even higher, so that in order for their global contribution to rival that of the velocity fluctuations it is sufficient that a fraction 0.1–0.5 of the total emission should come from such flows.

APPENDIX E: TOY MODEL OF SURFACE BRIGHTNESS PROFILES

To try and gain insight into the observed power spectra, we have determined the simplest emission model that can reproduce the qualitative features of regimes I–IV. The emission model is illustrated in Figure E1 and consists of the following spatial components:

(i) A narrow Gaussian with peak brightness 800 (±30%) and FWHM 4″ (±30%).
(ii) A broader Gaussian with peak brightness 400 (±30%) and FWHM 12″ (±30%).
(iii) A very broad Gaussian with peak brightness 240 (±30%) and FWHM 88″ (±50%).
(iv) A sinusoidal variation with wavelength 5″ (±50%) and relative amplitude 15%, which multiplies the sum of components (i)–(iii).
(v) Poisson $\sqrt{N}$ noise, assuming that the brightness is in units of counts/pixel.

The wavenumber $k = 1/\lambda$ of each component is indicated by vertical lines on the power spectrum shown in the upper panel of Figure E1 (dashed lines for the Gaussian components (i)–(iii), dotted lines for the sinusoidal component (iv)). For the Gaussian components, we assume $\lambda \approx 2 \times$ FWHM since the Gaussian peak represents only half of a fluctuation wavelength.

Components (i) and (ii) are chosen so as to reproduce regime II in the power spectra of § 3.1, with a relatively shallow slope ($\gamma > -3$) between scales of 8″ and 22″. As is, the model best represents the [N II] power spectrum (upper right panel of Fig. 5), but the precise value of the slope can be controlled by varying the relative strength of the narrow (4″) and the broader (12″) component. For example, the [O III] power spectrum requires nearly equal amplitudes for these two components.

With only components (i) and (ii), the model power spectrum is too shallow in regime I (with $\gamma \approx 0$) and is too steep in regime III, showing a deep minimum in the $k^3P(k)$ curve before arriving at the noise-dominated regime IV. These minor deficiencies are ameliorated by the introduction of the secondary components (iii) and (iv), respectively.

The average power spectrum from 100 realizations of the toy model is calculated, where the brightness and width of each component is chosen according to normal distributions with central value (± RMS % variation) as given above. The result is in remarkably good agreement with the observed power spectra, except that the observations tend to show sharper breaks at the boundaries between the different regimes. It should be emphasized that the toy model is only an idealization of the spatial variations present in the real surface brightness maps, which typically show ∼ 10 prominent peaks in each one-dimensional slit profile, rather than the single peak of the model.

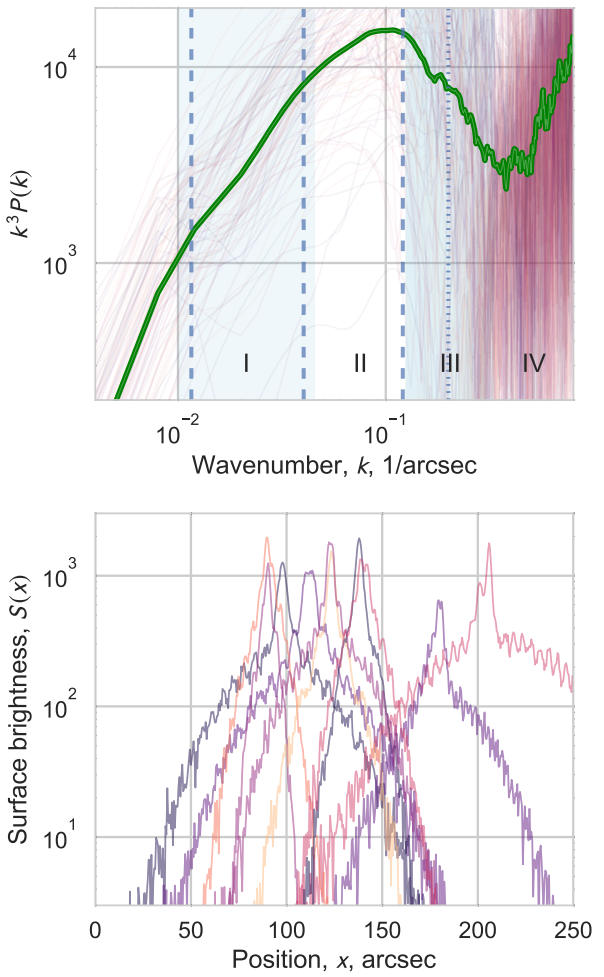

Figure E1. Compensated power spectra (upper panel) of 100 fake one-dimensional surface brightness profiles. Individual power spectra are shown as faint lines, while the the thick green line shows the average spectrum. The lower panel shows an example of 10 of the brightness profiles on a semi-logarithmic scale.

REFERENCES

Bertoldi F., McKee C. F., 1990, ApJ, 354, 529
Brunt C. M., Federrath C., Price D. J., 2010, MNRAS, 405, L56
Dyson J. E., 1968, Ap&SS, 1, 388
Henney W. J., Arthur S. J., de Colle F., Mellema G., 2009, MNRAS, 398, 157
Konstandin L., Girichidis P., Federrath C., Klessen R. S., 2012, ApJ, 761, 149
Konstandin L., Schmidt W., Girichidis P., Peters T., Shetty R., Klessen R. S., 2015, preprint, (arXiv:1506.03834)